Flow Turbulence Combust (2013) 90:471–490
DOI 10.1007/s10494-012-9427-7

Flow Field Around Single and Tandem Piers

Behzad Ataie-Ashtiani · Abolfazl Aslani-Kordkandi

Received: 23 October 2011 / Accepted: 5 November 2012 / Published online: 27 December 2012

Abstract The present study provides a comparison between the flow pattern around two circular piers in tandem and a single pier set up on a moderately rough flat bed in a laboratory flume. Velocities are measured by an Acoustic Doppler Velocimeter (ADV). The contours of the time-averaged velocity components, Reynolds shear stresses, turbulence intensities and turbulence kinetic energy at different planes are presented. Streamlines and vectors are used to study the flow features. The analysis of power spectra around the piers is also presented. The results show that the presence of downstream pier changes the flow structure to a great extent, particularly in the near-wake region. Within the gap between the two piers, a stronger and substantial upflow is shaped. However, a weaker transverse-deflection is formed in comparison with that in the single pier. Near the bed, the velocity of flow approaching the downstream pier decreases to 0.2–0.3 times of the approach mean velocity (U_0) due to the sheltering effect of the upstream pier. In the wake of downstream pier, the flow structure is completely different from the one in the wake of single pier. In comparison with the single pier, the values of turbulence kinetic energy and turbulence intensities show a considerable decrease around the tandem piers. In tandem piers, the high values of turbulence characteristics are found near the downstream pier. There is a recirculation zones just upstream of the sheltered pier close to the bed and another behind that pier near the free surface. The results show a decrease

B. Ataie-Ashtiani · A. Aslani-Kordkandi
Civil Engineering Department, Sharif University of Technology,
P.O. Box 11155-9313, Tehran, Iran

B. Ataie-Ashtiani
e-mail: ataie@sharif.edu

A. Aslani-Kordkandi (✉)
Faculty of Payam Noor University of Qeshm,
P.O. Box 79516-15991, Qeshm, Hormozgan, Iran
e-mail: aslani.abolfazl@gmail.com

in the strength of vortical structure in the wake of tandem piers in comparison with single pier. It is shown that the formation of flow with different Reynolds number along the flow depth due to the effect of bed roughness, as well as pier spacing, can influence the type of flow regime of tandem case. In addition to enhancing the flow structure indulgence, the present detailed measurements can also be used for verification of numerical models.

Keywords Flow pattern · Single pier · Tandem piers · Turbulence · Vortex shedding

1 Introduction

The estimate of the maximum possible scour around a bridge pier is necessary for the safe design of bridges. A large number of studies have been conducted to predict the scour depth around piers [e.g. 10, 11, 33]. Based on these studies, semi-empirical equations are available for the maximum scour depth. A lingering concern is that most of these equations are over-predicting the maximum scour depth for field, or even for laboratory conditions [5, 16, 32]. Understanding of the complex flow field and erosion mechanisms can provide a way out this problem. A comprehensive understanding of the turbulent flow structure can provide more insight into the scouring process and aid to predict scour depth precisely [1, 17]. For a better understanding of the flow pattern and turbulent flow around piers, many researchers have focused on the flow around piers with and without a scour hole [1, 15–18, 20, 21, 25, 26, 29, 43]. Most of these studies are related to single piers and provide detailed information on the flow around them. Due to geotechnical and economical reasons, pile groups and complex piers have become popular in bridge design [6, 14]. However, the direct application of the results derived for a single pier may be problematic [28]. Despite a large number of investigations around single piers, a comprehensive understanding of flow around pile groups and complex piers is still lacking.

In this study one of the simplest arrangements of pile groups, i.e. tandem arrangement, is studied. For this arrangement, several laboratory studies have been carried out to investigate the relation between the pier spacing and maximum scour depth [5, 22, 40]. Hannah [22] investigated scour depths around this arrangement for different spacing between the piers. Salim and Jones [40] observed that the scour depth decreases as the spacing between the piers increases. Ataie-Ashtiani and Beheshti [5] conducted experimental investigations of the scour around pile groups, especially two piers in tandem and provided a correction factor to improve the accuracy of the existing equations for prediction of the scour-hole maximum depth. Some researchers have provided or improved semi-empirical equations for pile groups and compound piers similar to those for the single piers [6]. A number of researchers performed several qualitative flow-visualizations to investigate the effect of pile spacing on the vortex shedding frequencies [23, 36, 38, 44]. Classifications of qualitative flow regime of tandem cylinders have been presented by Igarashi [23] and Zdravkovich [48]. Based on their descriptions, one can classify the flow around two-in-tandem cylinders in four types including: (i) the extended-body regime (single-slender-body regime), where the two cylinders are so close to each other that the free shear layers separated from the upstream cylinder overshoot the downstream

one, and the flow in the gap of the cylinders is stagnant; (ii) the reattachment regime (quasi-steady reattachment regime), where the shear layers separated from the upstream cylinder reattach on the downstream cylinder and the flow in the gap is still insignificant; (iii) the co-shedding regime (binary vortex street), where the shear layers roll up alternately in the gap between the cylinders and thus the flow in the gap is significant [29]; and (iv) bistable (unstable region) flow changing alternatively between a reattachment regime and a co-shedding one.

Palau-Salvador et al. [38] conducted numerical simulations around two submerged piers in tandem and presented flow streamlines at different planes. Mahjoub et al. [30] conducted flow visualization and velocity measurements around single pier and two submerged piers in tandem at two different spacing using PIV in wind tunnel to investigate near-wake region structures. They also presented profiles of important flow quantities such as velocities and Reynolds stresses at various planes.

So far, the studies of flow field around two piers in tandem are mainly confined either to the wake region or submerged piers situated on a smooth flat bed, and the effects of these flow characteristics on the bed sediments and vice versa have not been investigated. To our knowledge, contrary to the single piers, there is not a detailed study of flow field and turbulent characteristic around two partially submerged tandem piers.

The main objective of the present study is to carry out a detailed experimental investigation of the flow pattern around a tandem arrangement in a moderately rough flat bed in order to provide a better understanding of the three-dimensional flow. In order to have a reference study, the experiments have also been conducted around a single pier. The experiments were conducted under clear water conditions. All the measurements were taken by an Acoustic Doppler Velocimeter (ADV). The contours of the time-averaged velocity components, turbulence intensities, Reynolds shear stresses and turbulence kinetic energy at different horizontal and vertical planes are presented. Streamlines and velocity vectors obtained from the velocity fields are used to study the details of flow features. Furthermore, the analysis of power spectra around the piers is performed. Besides providing insight into the flow anatomy, the experimental data of this study can also be used for validation of numerical models. This study is the first part of a more extensive study of scouring around tandem piers, here with a fixed bed, i.e. without scour.

2 Experimental Setup and Procedures

The experiments were conducted at the Hydraulics Laboratory of the Civil Engineering Department of the Sharif University of Technology, Tehran, Iran. Experiments were carried out for single and tandem piers in two different channels (Fig. 1). However, both experiments had similar hydraulic conditions. The bed was fixed to prevent scour hole development. As the study of scour development is considered in the future experiments, the size of the channels and other dimensions were adopted so that they can satisfy the universal criteria for scouring experiments. The criteria are as follows:

1. The ratio of the channel width to the pier diameter should be greater than 6.5 so that the channel wall has no effect on the scouring dimensions.

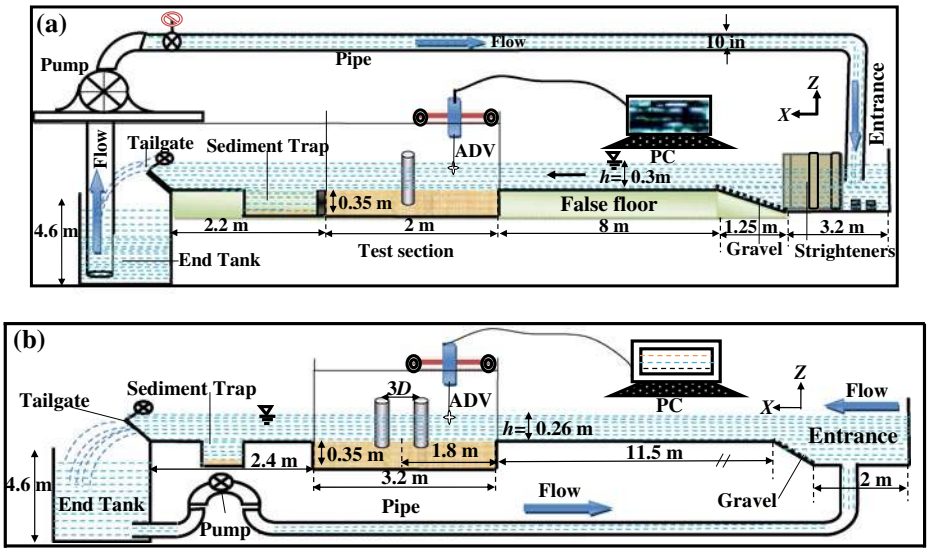

Fig. 1 Side view of experimental models **a**: single pier, **b**: tandem piers (not to scale)

2. The ratio of the flow depth to the pier diameter should be greater than 3–4 so that the scour depth is independent of the flow depth.
3. The ratio of the pier diameter to the median size of the sediment grain, d_{50}, should be greater than 50 so that the size of sediment particles has no influence on the scour depth [31].

In addition, the diameter of the pier was adopted about 10 times larger than the diameter of the probe so that the probe did not have undesirable influences on the flow pattern [18]. These criteria should be satisfied for all stages of the scouring processes. As mentioned already, this paper is focused on the flow field before occurrence of the scouring and fixed flat bed is used for both experiments in this study.

For the tandem-pier experiment (Fig. 1b), a false floor was placed at the bottom of the channel. A 3.2-m long and 1.5-m wide recess was placed at a distance of 13 m from the entrance of the channel, to allow the flow to become fully developed. The piers were placed in the recess and then the recess was filled with uniform sand and finally the bed was leveled carefully. As shown in Fig. 2 the two nylon-made piers

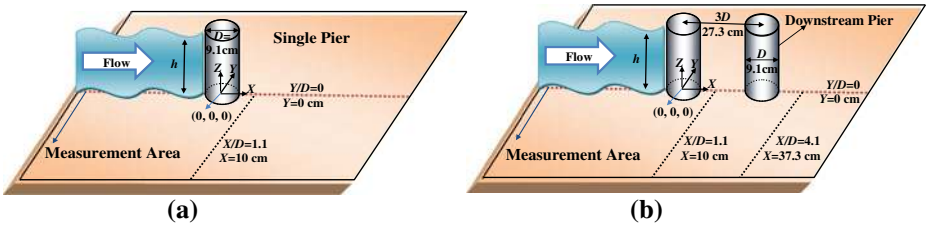

Fig. 2 3-D view of test sections, measurement sites and definition of variables **a**: single pier **b**: two piers in tandem

had center-to-center distance (G) of 273 mm or 3.D. For the single-pier experiment, a 2-m long and 1.26- m wide recess was placed at a distance of 10 m from the entrance (Fig. 1a).

To prevent sediment motion, the top layer of the recess was frozen by spraying synthetic glue. The synthetic glue mixed with water (1:3 by volume) was sprayed uniformly over the bed. After 72 h, the synthetic glue was set and the bed was stabilized. This glue has no undesirable effects on the sediment [4].

The uniform sand used in both experiments at the bed of the test section was glued over the false floor to simulate turbulent flow over a moderately rough flat wall. A water discharge of 134 lit/s was generated by the pump installed near the end of the water reservoir. The channel was slowly filled with water from the downstream side before the pump starts to work in order to prevent any damage to the channel bed. The flow depth in the flume was regulated using a tailgate. At the entrance of the channel an oblique floor with gravel surface was placed to prevent the formation of large-scale disturbances. Table 1 shows the hydraulic conditions and the characteristics of the experimental models.

Both experiments were carried out for conditions slightly lower than the threshold condition for sediment motion at the test section (i.e., $u^*/u_c^* \approx 0.95 - 1$), where u^* ($= 0.018$ m/s) is the bed shear velocity computed from the measured velocity profile at the upstream approach flow and u_c^* ($= 0.019$ m/s) is the critical bed shear velocity calculated using the method proposed by of Beheshti and Ataie-Ashtiani [8]. The method of the maximum of the $\overline{u'w'}$ Reynolds shear stress also gives u^* close to 0.018 m/s. The threshold condition is further related to the scouring criterion and it is mentioned here due to aforesaid reasons. Owing to differences in the size of the two channels, in order to achieve the near-threshold condition, water depths of 30 and 26 cm with the approach mean velocities (U_0) of 0.354 and 0.346 m/s were adopted for the single and tandem piers experiments, respectively. Reynolds numbers, based on flow depth and pier diameter, were approximately 10^5 and 3×10^4, respectively, and the Froude number was 0.22, showing a turbulent and subcritical flow.

The roughness Reynolds number $\left(Re^* = u^* K_s / \nu\right)$ is equal to 12.78 where ν is the kinematic viscosity. Here, the equivalent roughness height K_s quantifies the influence of roughness elements. For stationary flat beds in laboratory experiments, K_s is usually set to the median diameter d_{50} of bed material (as in this study) because there is only sand-grain roughness on the bed [47].

The instantaneous three-dimensional velocity components were measured by a NorTek made 5-cm ADV [35]. The ADV operates on a pulse-to-pulse coherent Doppler shift to provide instantaneous three-dimensional velocity components at

Table 1 Characteristics of the two experiments where Q is the discharge, h is the flow depth, Re(D) is the Reynolds number based on the pier diameter, Re(h) is the Reynolds number based on the flow depth, Fr(h) is the Froude number, L is the channel length, b is the channel width, D is the pier diameter, d_{50} is the median size, Ss is specific gravity, σ_g is geometric standard deviation of sediment particles and U_0 is the depth-averaged approach-flow velocity

	Q (Lit/s)	h (m)	$Re(D)$	$Re(h)$	$Fr(h)$	L (m)	b (m)	D (cm)	d_{50} (mm)	S_s	σ_g	u^*/u^*c	U_0 (m/s)
Single pier	134	0.3	3.2×10^4	1.06×10^5	0.21	15	1.26	9.1	0.71	2.45	1.2	0.95–1	0.354
Tandem piers	134	0.26	3.1×10^4	0.9×10^5	0.217	17	1.50	9.1	0.71	2.45	1.2	0.95–1	0.346

a rate of 25 Hz. The rate of 25 Hz also was used in the measurements of Nikora and Goring [34], Song and Chiew [41], and Ge et al. [19]. An instrument carriage was mounted on top of the flume which was able to move in both longitudinal and transverse directions as well as in the vertical direction. The 3-D down-looking probe of the ADV was unable to measure the velocity in approximately the upper 5 cm of the water column and in the zone closer than 3.9 cm to the pier. Hence, this probe was used in combination with a 3-D side-looking and up-looking probe to measure more points close to the piers and the free water surface. Measurements in the zone closer than 4.5 mm to the boundary (bed or pier surface) were beyond the ability of the ADV.

Because of the interference due to echoes from the bed, the received signal might have been disturbed, which may result in inaccurate velocity measurement [41]. In the present study a few points which suffered from this problem were found in a zone located at about 2.9–3.8 cm above the bed. The same noise problem was also reported by Carbonneau and Bergeron [13], Snyder and Castro [42] and Beheshti and Ataie-Ashtiani [9]. The unrealistic data were eliminated after inspecting the time series [4].

The ADV has minor interference with the flow-field, as the measurement samples were positioned about 5 cm away from the probes. Using the stationary analysis, the sampling durations were varied from 120 to 250 s in order to achieve a statistically independent average velocity. Ge at al. [19] adopted a smaller time duration equal to 120 s. Buffin-Bélanger and Roy [12], by determining standard errors of turbulence statistics obtained from velocity measurements in fluvial turbulent boundary layers, showed that, for most turbulence statistics, the optimal record length (minimum sampling effort to achieve low standard errors) ranged between 60 and 90 s.

The measurements in these experiments were taken in a Cartesian coordinate system (X, Y, Z) referring to streamwise, transverse and vertical directions respectively, with time-averaged velocity components (u, v, w) and corresponding velocity fluctuations (u', v', w'). The origin of the Cartesian coordinate system for the single pier and the two tandem piers was centered at the base of the pier and the upstream pier, respectively, as shown in Fig. 2.

The measurements were only carried out on one side of the plane of symmetry $(Y/D = 0)$. Measurements were taken at both horizontal and vertical planes. The horizontal planes were located near the bed ($Z/h = 0.02$ and 0.027 for single-pier and two-pier cases, respectively) and near the middle of the flow depth ($Z/h = 0.54$), in order to show the flow behavior at the area close and far from the sediment bed, respectively. The vertical planes were the plane of symmetry $(Y/D = 0)$ and the transverse planes located at $1.1D$ downstream of the pier center, as shown in Fig. 2. A total number of 1270 and 1500 point-velocity measurements were made for single and two-pier experiments, respectively. All data were processed using the public domain software WinADV (Wahl, [45]) to obtain the time mean and Root Mean Square (RMS) values of each point-velocity record. The measurements were filtered using this software to eliminate points having a correlation coefficient less than 0.70 and SNR (Signal-to-Noise Ratio) less than 15. Furthermore, data obtained from ADV was filtered using the spike removal algorithm after Wahl [46]. The experimental uncertainties were estimated to have 99 % confidence level using the method provided by Kline [27]. Uncertainties for velocities and turbulence intensities were 1 % and 2.5 % respectively. These uncertainties were greater in the wake region. Having corrected the velocity data obtained from raw data, the three mean-velocity

components (u, v, w), turbulence intensities as standard deviations of the instantaneous three-dimensional velocity components $\left(u^+ = \sqrt{\overline{u'^2}}, v^+ = \sqrt{\overline{v'^2}}, w^+ = \sqrt{\overline{w'^2}}\right)$, Reynolds shear stresses $\left(-\rho\overline{u'v'}, -\rho\overline{u'w'}, -\rho\overline{v'w'}\right)$ (where ρ is mass density of water) and turbulence kinetic energy $K = 0.5\left(u^{+2} + v^{+2} + w^{+2}\right)$ were calculated based on the results [4].

3 Results and Discussions

The values of velocity components and turbulence intensities were normalized by U_0; the values of Reynolds shear stresses and turbulence kinetic energy were normalized by U_0^2. Further, vertical elevations and horizontal distances were normalized by h (flow depth) and D (pier diameter) respectively. Therefore, all the presented results are non-dimensional.

3.1 Inlet flow condition

The inlet condition of the flow is presented by velocity profiles of the approaching flow far upstream of the single pier and the two tandem piers. As shown in Fig. 3a, the profile of u/U_0 demonstrates that the flow is fully developed and the inlet velocity profiles of the two experiments are similar in value and distribution. The profiles v/U_0 and w/U_0 (Fig. 3b and c) show that the flow deflection in vertical and transverse

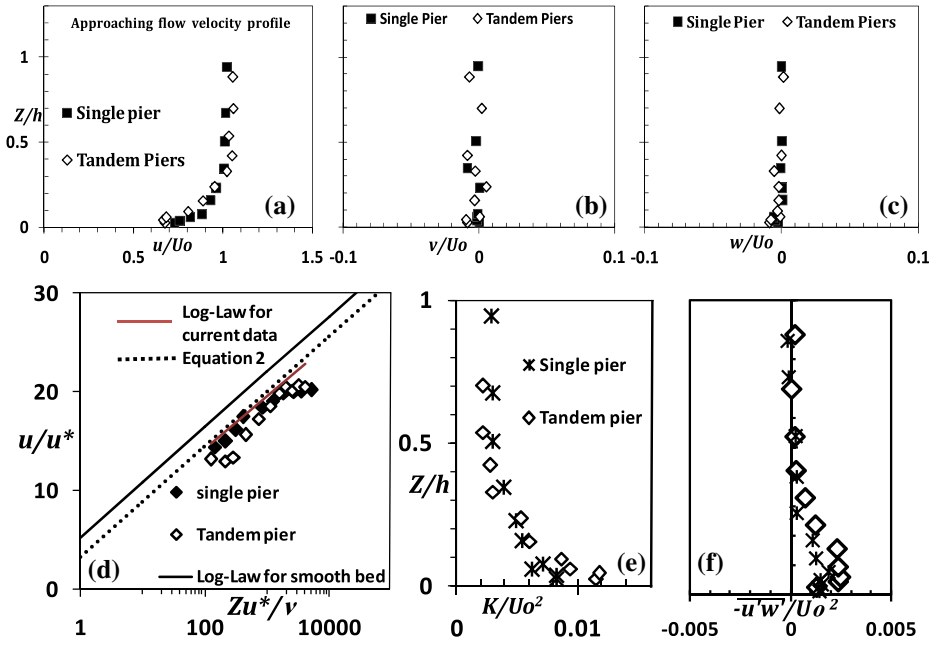

Fig. 3 Approach- flow velocity profiles of the three components: u(**a**), v(**b**), w(**c**); clauser plot of u-profile (**d**), turbulent kinetic energy k (**e**), Reynolds shear stress $u'w'$(**f**)

directions is negligible. The measured profiles of the stream-wise velocity compared with the log-law (Fig. 3d), turbulent kinetic energy (Fig. 3e) and Reynolds shear stress (Fig. 3f) are also presented for both experiments. The log-law for rough walls reads:

$$u/u^* = \frac{1}{k}\, ln\left(\frac{Z u^*}{\nu}\right) + B - \Delta B \tag{1}$$

where k is Von Karman's constant ($\approx$0.41) and B is a constant ($\approx$5.2) And ΔB is the downshift of the log-law profile due to roughness effects ($\Delta B = 0$ for smooth walls). ΔB is a function of roughness, Reynolds number, Re^*, and for intermediate roughness ($2.25 \leq Re^* < 90$), Wu et al. [4] gave the following relation:

$$\Delta B = \left[B - 8.5 + \frac{1}{k}\, ln\, Re^*\right] \sin\left[0.4258\left(ln\, Re^* - 0.811\right)\right] \tag{2}$$

The resulting log-law (and also the smooth-wall log-law with $\Delta B = 0$) is plotted in Fig. 3d and compared with the log-law fitted through the experimental data. The agreement can be seen to be good and the downshift due to roughness can also be clearly seen. For the present experimental setup ($Re^* = 12.78$), ΔB according to this relation is about 2.

3.2 Flow field in horizontal planes

In this section, the results for both experiments are presented on one side of the plane of symmetry. Figure 4 shows streamlines at two levels for both cases. According to Fig. 4, behind the single pier, a region having reverse flow and strong rollers is found and its length increases as the distance from the bed increases. At the upper level, the reverse-flow region ends at the distance approximately 0.5D farther downstream than at the lower level. The centers of the foci in the wake region move further downstream from the piers as the level increases. The experimental results of Sahin et al. [39] also show this behavior. Near the bed, the attached boundary layer on the sides of the pier extends further downstream and this phenomenon consequently

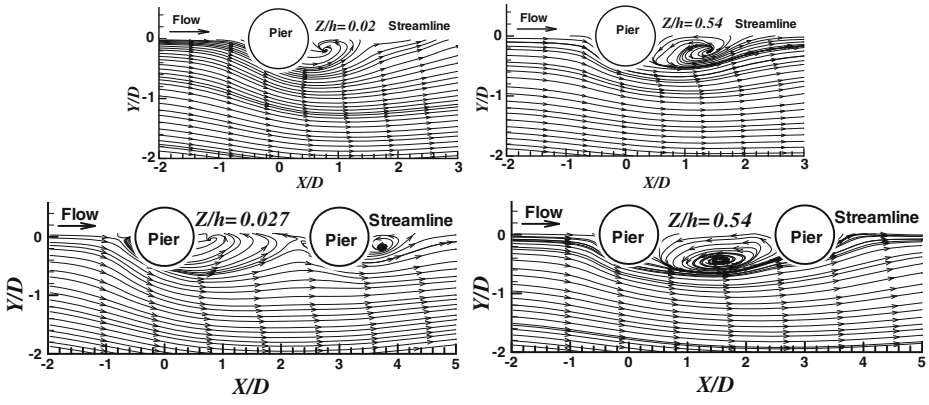

Fig. 4 Streamlines at two horizontal levels for both experiments; near the bed (*left*), and near the mid-depth (*right*)

results in a smaller wake in comparison to the upper level. This behavior is attributed to the effect of bed roughness on turbulence increase near the bed, so that the turbulent boundary layer on the sides of the pier is more resistant, and separation is delayed until the downstream side of the pier.

In the tandem-pier case, the behavior of flow upstream of the piers is similar to that in the single-pier case, but behind the piers this similarity decreases due to presence of the downstream pier. Near the bed and within the gap between the two piers, the reverse flow extends almost to the downstream pier after which the flow is again in the main-stream direction. In this region vortex shedding occurs partially. According to the aforementioned classification of the qualitative flow regime, the flow regime formed within the gap is termed co-shedding regime or binary vortex street. At the upper level, the shear layers separated from the sides of the upstream pier move further downstream and reach each other on the surface of the downstream pier. In this case, there is no vortex shedding within the gap. This type of flow regime is termed reattachment regime. It should be mentioned that the formation of flow with different velocities (different Reynolds number) along the flow depth due to the effect of bed roughness, as well as pier spacing, can influence the type of flow regime within the gap as reported by Zdravkovich [48].

In Figs. 5 and 6, contours of the three components of velocity at two horizontal levels around the piers are presented. Owing to the contraction of flow area at the sides of the piers, there is an increase in the value of u/U_0 (Fig. 5a). Since the wake is a recirculating zone that does not contribute to the net transport of fluid in the downstream direction, the flow in the region adjacent to the wake tends to

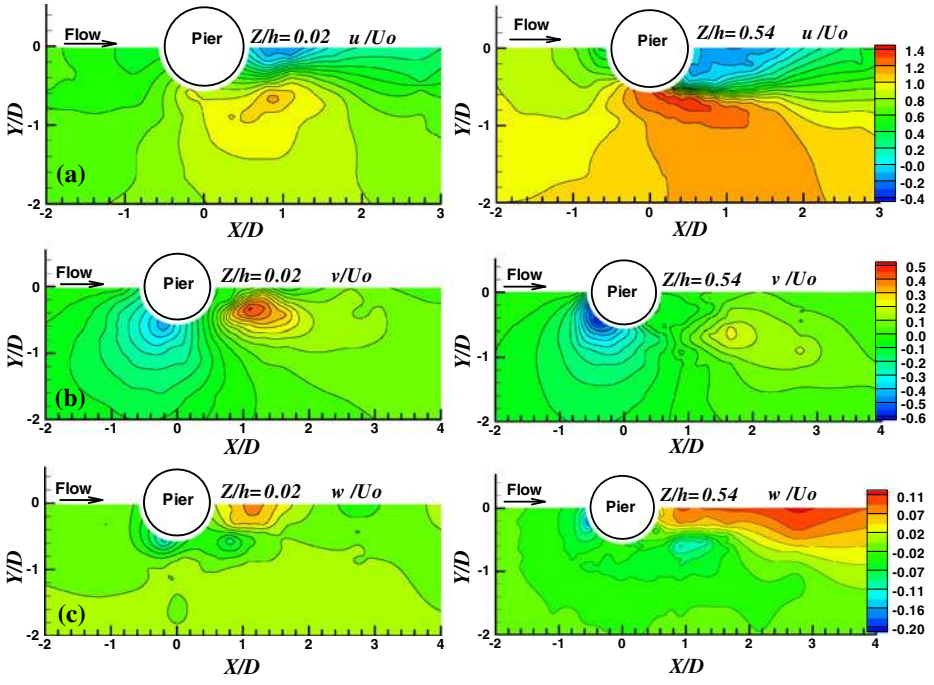

Fig. 5 Contours of the three components of mean velocity at two horizontal levels around the single pier **a**:u/U_0, **b**:v/U_0, **c**:w/U_0, (*right*): near the mid-depth, and (*left*): near the bed

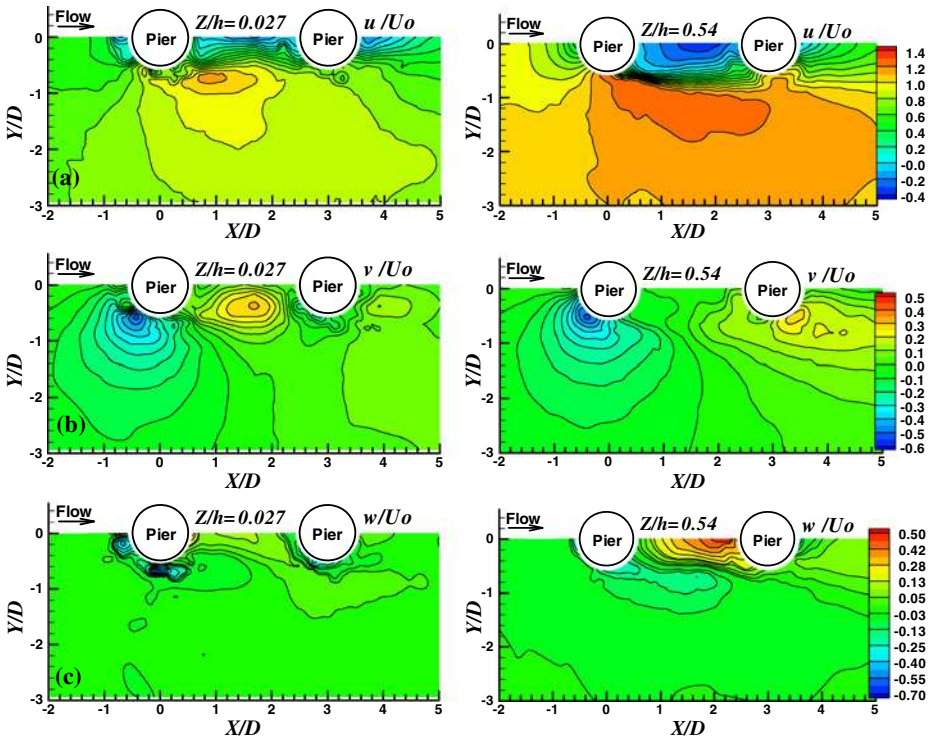

Fig. 6 Contours of the three components of velocity at two horizontal levels around the tandem piers **a**:u/U_0, **b**:v/U_0, **c**:w/U_0, (*right*): near the mid-depth, and (*left*): near the bed

accelerate in order to transport the extra fluid [1]. For the two piers in tandem (Fig. 6a), a reverse flow is seen throughout the gap between the two piers. Behind the downstream pier there is a stronger reverse flow near the bed than that at the upper level. This is related to the formation of new streamwise flow (co-shedding regime) in front of the downstream pier. The presence of the downstream pier makes the reverse flow region extend $1D$ further than that in the single-pier case. Due to the sheltering effect of the upstream pier, the velocity of the flow approaching the downstream pier decreases resulting in a smaller and weaker wake region behind this pier than that behind the upstream pier. The transverse velocity (v/U_0) in front of the single pier and at the upper level is stronger than that in the lower level due to the high velocity of the approaching flow (Fig. 5b). The intensity of the transverse deflection downstream of the pier is found to be inversely related to the size of the wake region. The transverse velocity changes inside the gap and downstream of the pier according to the flow regime formed around the two piers in tandem (Fig. 6b). Near the bed and inside the gap, the deflection of flow is obvious because in this area the shear layers separated from the piers curve towards each other. In contrast, at the upper level there is no such high deflection inside the gap because in this region the shear layers do not reach each other, while near the downstream pier and on the sides of it, they attach to the pier and the values of v/U_0 become comparable with those in the gap at the lower level. In the single-pier case, the flow deflects towards the bed due to difference in the pressure along the flow depth upstream of

the single pier (Fig. 5c). In the wake of the pier, an upward flow is found around which a down flow is formed to ensure continuity. In the two-pier case, similar to the single-pier case, a downflow is seen in front of the upstream pier (Fig. 6c). There is a remarkable upflow in the gap in comparison with relatively weak upflow behind the single pier. Near the bed, this flow encounters resistance of the downflow created in front of the downstream pier and cannot develop. This interaction may also prevent the horseshoe vortex formation at the base of downstream pier. Behind the downstream pier, there is no vertical deflection. At the upper level and between the two piers, the upward flow is dominant and this flow reaches its maximum value near the downstream pier. Behind this pier instead of common characteristic of wake region, a relatively small downflow is found.

3.3 Flow field in vertical planes

Figure 7 shows streamlines and velocity vectors for both experiments in the vertical plane of symmetry. In this figure, the magnitude and direction of velocity vectors are $\left(u^2+w^2\right)^{0.5}\Big/U_0$ and Arctan (w/u) respectively. In addition, the magnification of the flow features in front of the upstream and downstream piers is presented in Fig. 8.

In the upstream region, the behavior of the approaching flow for both experiments is similar. According to the streamlines, particularly those in front of the upstream pier in Fig. 8a, there is a downward and reverse flow that is a horseshoe vortex at the base of the piers formed in a small region near the bed just upstream of the pier. According to Dargahi [15] and Ahmed and Rajaratnam [1], the point located at the end of this region is the primary flow separation point. Ozturk et al. [37] carried out experiments around a single pier for flow with Re(D) in the range 750 to 9500. They showed that as the Reynolds number increases the center of the horseshoe vortex shifts towards the base of the pier. As expected in this study, for Re(D) of about 3×10^4 the center of the horseshoe vortex is just upstream of the pier. This horseshoe vortex system travels downstream of the cylinder and mixes with the fluid

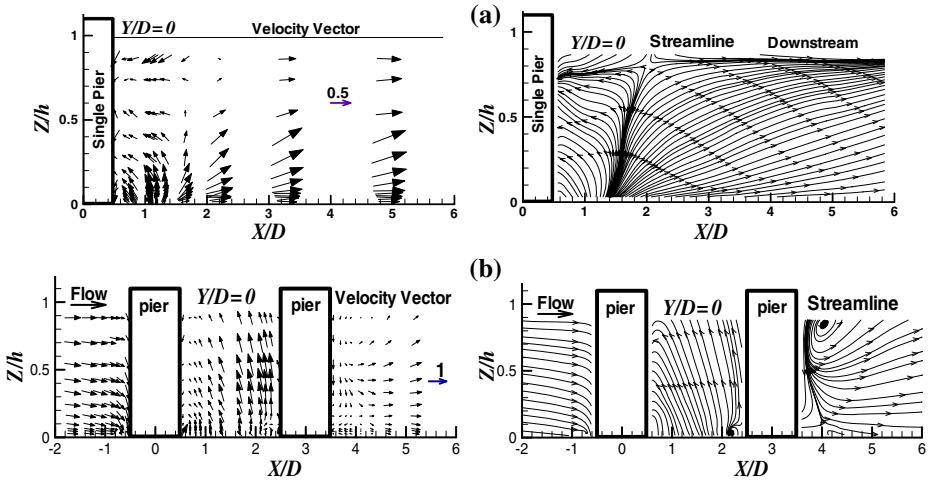

Fig. 7 Streamlines and velocity vectors in the plane of symmetry, **a**: single pier **b**: tandem piers

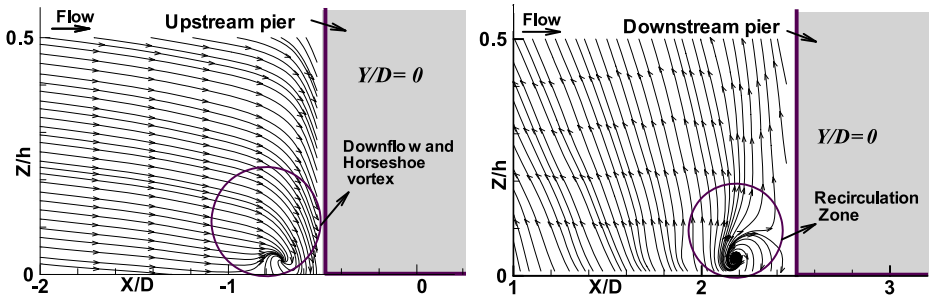

Fig. 8 Magnification of the flow feature upstream of each pier in the tandem-pier experiment

of the wake flow region. The interaction of this horseshoe vortex system with the bed generates further turbulence near the bed as stated by Sahin et al. [39].

Behind the single pier, in the wake of the pier, an upflow and a reverse-flow region are found, whose extent increases towards the free surface. This is in agreement with the experimental results of Sahin et al. [39]. The upflow has its maximum intensity near the line dividing the two regions having opposite flow (reverse and main stream) as shown in Fig. 7a. Between the two piers, the flow behavior changes noticeably and the upflow is found everywhere in the gap (reattachment regime) except near the bed just in front of the downstream pier (co-shedding regime). It seems that the presence of the downstream pier makes some pressure changes in the wake of the upstream pier and results in a further advance of shear layers in the downstream direction compared to that in the wake of the single pier. The velocity vectors reveal that the upflow in the downstream half of the gap is stronger than that in the upstream one. Near the bed and just in front of the downstream pier, a small recirculation is detected that is attributed to the change from the co-shedding regime to the reattachment one. As also seen in Fig. 8b, this type of flow structure cannot be a horseshoe vortex, because in this area the downflow is suppressed due to the formation of the reattachment regime.

A reserve flow is found between the two piers throughout the gap except for the region near the bed in front of the downstream pier. In this region (near the bed) the velocity of flow approaching the downstream pier decreases to $0.2–0.3U_0$ due to the sheltering effect of the upstream pier. On the other side, behind the downstream pier, the situation is very different from the characteristics typical for the wake of a single pier. Behind the pier a narrow area of downflow is observed and close to the free surface a recirculation zone is formed.

Figure 9 shows streamlines and velocity vectors in the transverse planes located at $1.1D$ downstream of the piers' center. In the single-pier case near the plane of symmetry, there is an upflow indicating the wake of the pier (Fig. 9a). Beside this flow, the flow is deflected towards the bed as well as towards the plane of symmetry to satisfy continuity. The interaction between this flow and the upflow emanating from the bed towards the water surface in the wake region make a circulation zone in front of the single pier. Approaching the bed, the intensity of downflow decreases but the intensity of transverse flow deflected towards the plane of symmetry increases. In the tandem-pier case, behind the upstream pier (Fig. 9b), the general features are similar to those at the single pier. However, at this section, the transverse flow deflection is just confined near the bed and a nearly uniform downflow is observed along

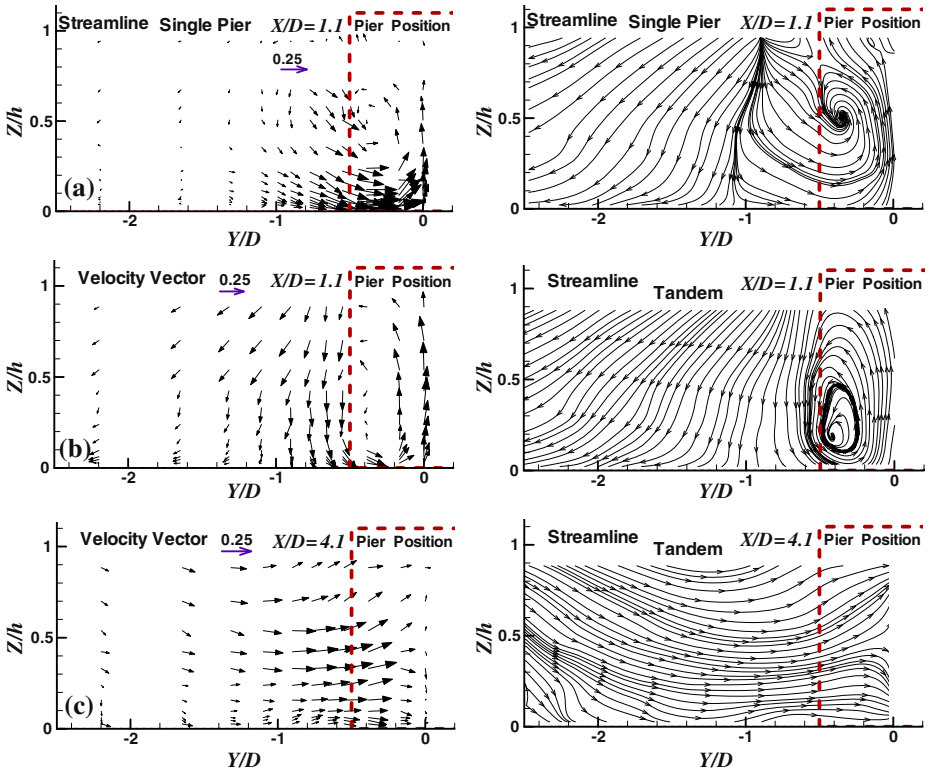

Fig. 9 Velocity vectors and streamlines in the transverse planes downstream of the **a**: single pier ($X/D = 1.1$), **b**: upstream pier ($X/D = 1.1$), and **c**: downstream pier ($X/D = 4.1$) in tandem arrangement

the flow depth. This phenomenon can be attributed to the expansion of the wake region in the entire gap and consequently to the controlling of the flow deflection. Behind the downstream pier ($X/D = 4.1$) (Fig. 9c), approximately throughout the transverse section, the flow converges to the plane of symmetry so that the flow nature is completely different from that in the two previous planes.

Figure 10 presents a simple sketch of the 3-D flow structure around the piers. When two circular cylinders are situated in close proximity to each other, the fluid behavior is more complex than in the case of the single, isolated circular cylinder.

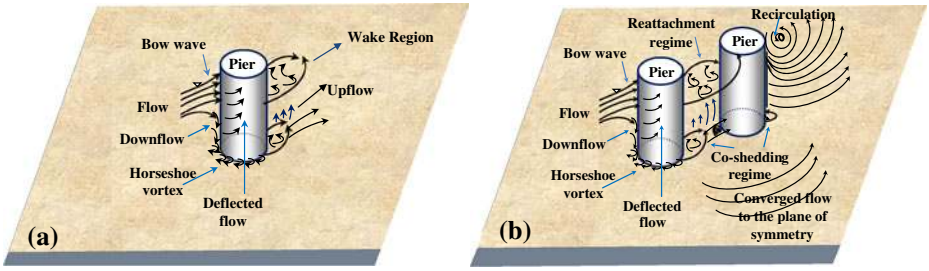

Fig. 10 Sketch of 3-D flow structure for **a**: single pier **b**: tandem piers

Flow in a channel, being a boundary-layer flow, approaches the cylinder and a stagnation pressure establishes itself. This will produce a (weak) pressure gradient along the front of the cylinder and induce a downward flow. Since there is also a pressure gradient around the cylinder, the downstream flow will be laterally diverted. Due to the stagnation pressure in front of the cylinder, the water surface rises, forming a bow wave [20]. The downflow and the surface roller (bow wave) formed in front of the upstream pier are similar to those in single piers. However, behind the upstream pier in the tandem-pier case (gap area), the separated shear layers move further in the downstream direction in comparison to the single-pier case. Behind the downstream pier in the tandem-pier case, except for the zone near the bed, the flow structure is significantly different from the one in the wake of the single pier.

3.4 Turbulence fields in horizontal planes

Contours of turbulence kinetic energy $\left(K/U_0^2\right)$ in two horizontal planes are shown in Fig. 11 for both cases. Behind the single pier, a core of the higher magnitude of K/U_0^2 is found in the wake of the pier due to the formation and shedding of very strong rollers. Around the tandem piers, the values of K/U_0^2 decrease to a great extent. These values are of the same order in the gap and behind the downstream pier near the bed. However, at the upper level, the values of K/U_0^2 are higher within the gap in comparison with those behind the downstream pier. It is remarkable that the downstream part of the gap area has higher turbulence kinetic energy than the upstream part. The flow anatomy around the two piers in tandem is different and more complicated in comparison with that in the single-pier case.

3.5 Turbulence fields in vertical planes

3.5.1 Turbulence intensities

Figure 12 illustrates the contours of turbulence intensities in the plane of symmetry for both experiments. The parameters u^+, v^+ and w^+ refer to values of turbulence intensities in the longitudinal, transverse and vertical directions, respectively. The

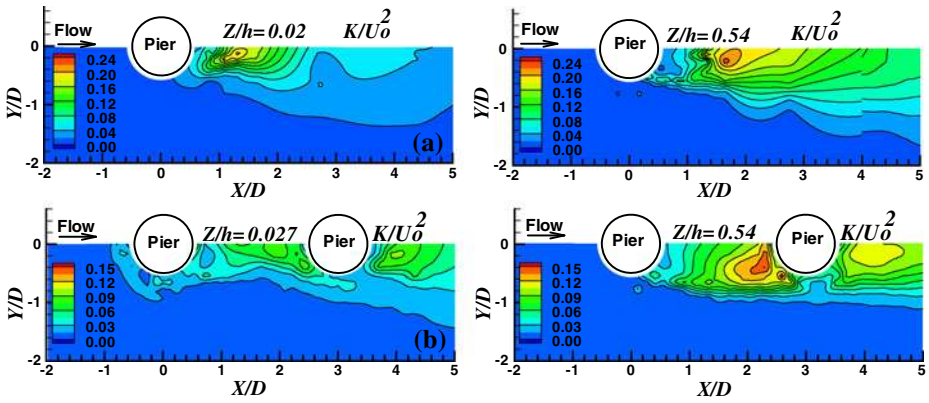

Fig. 11 Contours of turbulence kinetic energy around **a**: single pier **b**: tandem piers at two horizontal levels; (*right*): near the mid-depth, and (*left*): near the bed

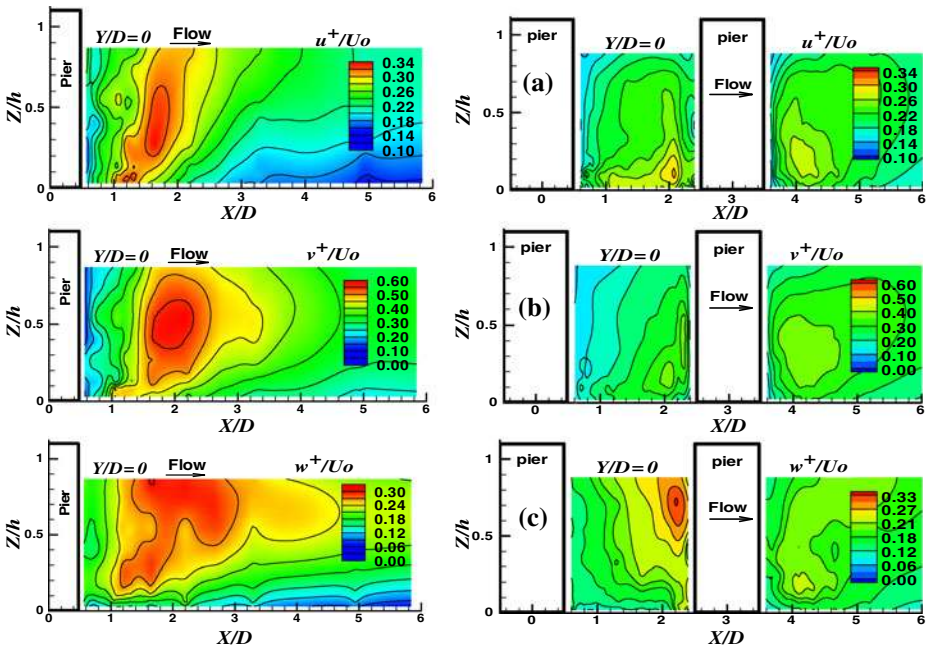

Fig. 12 Contours of turbulence intensities at the plane of symmetry for both experiments; **a**:u^+/U_0, **b**:v^+/U_0, **c**:w^+/U_0, (*right*): between and downstream of the two tandem piers, and (*left*): downstream of the single pier

behavior of turbulence intensities upstream from the pier for both experiments is similar (not shown here) and the results show that the values of turbulence intensities are negligible except near the pier and bed. Downstream from the single pier, turbulence intensities have maximum values around a distance of $2D$ from the pier center and a core of strong turbulence intensities is observed around this area coinciding with the region where the upflow velocity reaches its maximum values. Further downstream of the pier, the turbulence intensities decrease to their minimum values. According to this figure, the values of v^+/U_0 are much larger than u^+/U_0 and w^+/U_0, reaching a maximum value of 0.6, which is almost twice as large as that for the two other turbulence intensities. This situation is attributed to the fact that the shed vortices are associated with very large transverse fluctuations.

Between the two piers, the high values of u^+/U_0 are found near the bed and close to the downstream pier. The values of v^+/U_0 show a considerable decrease between the two piers as well as behind the downstream pier so that the maximum value decreases to about 0.66 times of values in the single pier. A core of high w^+/U_0 is formed above the mid depth just in front of the downstream pier coinciding with the region having strong upflow. As can be seen in the tandem-pier case, the high values of turbulence intensities occur close to the downstream pier and similar to the results of the turbulence kinetic energy, these values are smaller than those in the single-pier case.

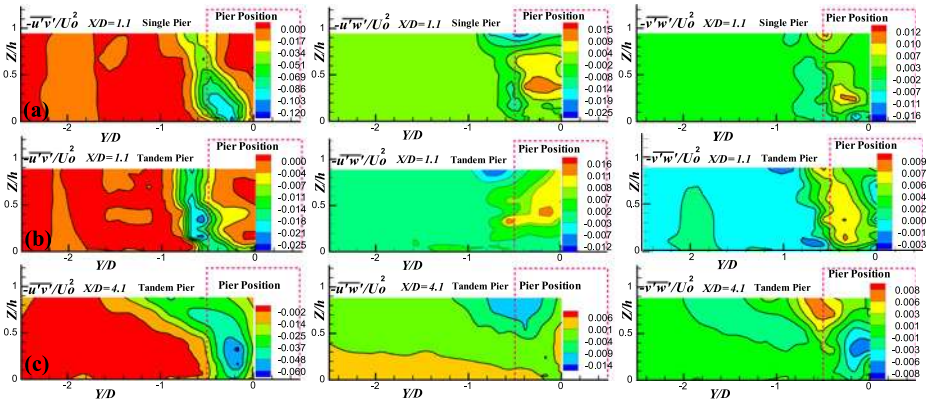

Fig. 13 Contours of Reynolds shear stresses in the transverse planes downstream of the **a**: single pier ($X/D = 1.1$), **b**: upstream pier ($X/D = 1.1$), and **c**: downstream pier ($X/D = 4.1$) in tandem arrangement

3.5.2 Reynolds shear stresses

Reynolds shear stresses are used in calculating the bed shear stress and their analysis is a subject of interest to engineers and scientists because of their significance in the formation of a scour hole. Figure 13 shows the contours of Reynolds stresses in the transverse planes located at $1.1D$ downstream of the piers' center. In this figure, the values of Reynolds shear stresses were normalized by ρU_0^2. In the single-pier case, approaching the plane of symmetry, the absolute values of the $-\overline{u'v'}/U_0^2$ component increase as a result of separation of the shear layers as well as the formation and shedding of very strong rollers downstream of the pier. These values are stronger behind the single pier than those behind the two tandem piers. Contrary to the planes $X/D = 1.1$ in both experiments, in the plane $X/D = 4.1$, there is not any region of large $-\overline{u'v'}/U_0^2$ value behind the downstream pier. The values of $-\overline{u'w'}/U_0^2$ and $-\overline{v'w'}/U_0^2$ also increase near the wake region, but in comparison with the values of $-\overline{u'v'}/U_0^2$ have a small growth. Figure 14 shows the contours of Reynolds shear stresses in the plane of symmetry between the two tandem piers. As seen in this figure, the absolute values of $-\overline{u'v'}/U_0^2$ are mainly small except close to the downstream pier where these values show a considerable increase like the other turbulence characteristics (i.e. turbulence intensities and kinetic energy). The values of $-\overline{u'w'}/U_0^2$ also increase in the downstream direction towards the water surface. Similar to these two components, the values of $-\overline{v'w'}/U_0^2$ increase near the downstream pier. This situation is mainly related to the shear layers separated from the upstream pier that reach each other at the downstream pier.

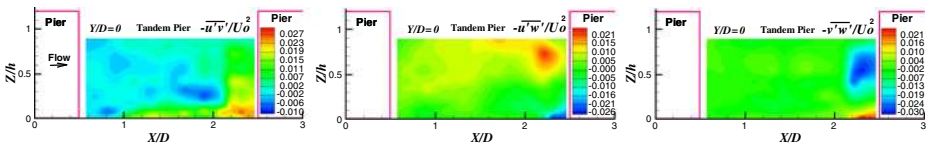

Fig. 14 Contours of Reynolds shear stresses at the plane of symmetry between the two piers

3.6 Frequency and intensity of shed vortices

Powerspectrum analysis of the instantaneous-velocity measurements at different points in the wake of the piers was conducted in order to find the dominant vortex-shedding frequency of the large-scale coherent structures. Power spectrum at each point was calculated using Fast Fourier Transformation (FFT) of the auto-covariance function of velocity time-series data. For both cases and at two levels the power spectra, $S(f)$, are shown in Fig. 15, and they are the resultant of the power spectra of the three components of flow velocity. The position given in the legend of individual figure parts indicates the points where $S(f)$ is maximum. The power associated with the peak frequency of the power-spectrum distribution indicates the strength of vorticity of wake vortices formed by the cylinder. The strength of wake vorticity expresses the capacity of wake vortices to entrain and move bed sediment from the flanks and rear of each cylinder (Ettema et al. [18]). The results show a decrease in the strength of vortical structure in the wake of tandem piers in comparison with single pier. According to Fig. 15, contrary to the two piers in tandem, in the single-pier case there is a clearly distinguishable power spectrum at each level with a substantial value of $S(f)$, twice as large as that of two piers at the equivalent levels. This state of affairs is attributed to the effect of two piers on distributing the maximum value of $S(f)$ and making it alter into some smaller values. Therefore, it can be concluded that in comparison to the two piers in tandem behind the single pier the high value of $S(f)$ shows a high capability of sediment entrainment. The results derived from FFT (not shown here) show that in the tandem case and near the bed due to the formation of a co-shedding regime, the two circular piers shed vortices separately at the same frequency. This is in agreement with the result reported by Mahbub Alam and Zhou [29]. For the two tandem piers, the sampling duration (120–250 s) covers about 60 to 125 shedding cycles; therefore, the vortex shedding

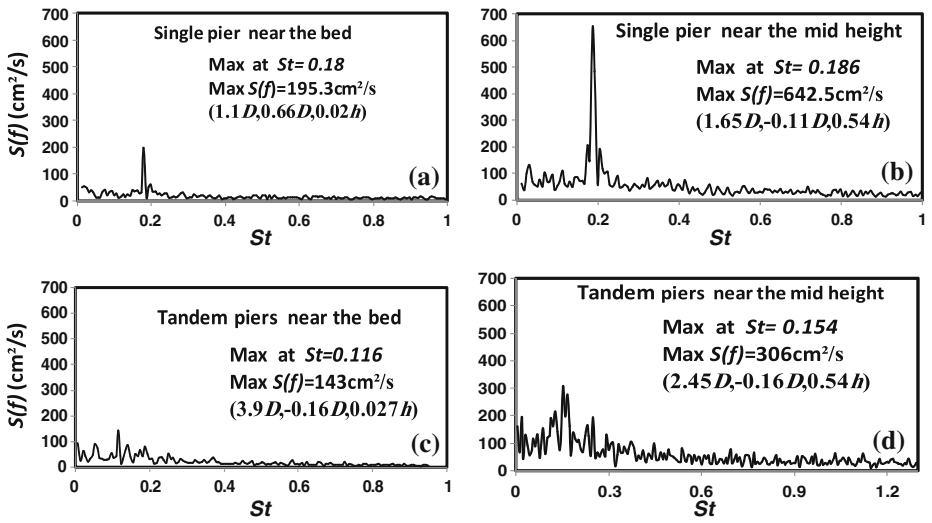

Fig. 15 Power spectra at the two horizontal levels for the two experiments; **a**, **b**: single pier, **c**, **d**: tandem piers, **b**, **d**: near the mid-depth, and **a**, **c**: near the bed

frequency (f) is about 0.5 Hz which in terms of the Strouhal number, $St = fD/U_0$; is approximately 0.13. For the single-pier case, the Strouhal number is 0.186 near the mid depth which is close to the findings of Ettema et al. [18]. Near the bed, this value is slightly smaller than that near the mid depth. Akilli et al. [2] and Akilli et al. [3] reported Strouhal number equal to 0.21 for single piers. Bearman and Wadcock [7] and Kim and Durbin [24] found St equal to 0.2 for single piers on a smooth bed. Igarashi [23] for the Reynolds number based on the pier diameter 2.2×10^4 and 3.5×10^4, reported St equal to 0.15 for the two piers in tandem. For the tandem piers in this study, near the mid depth the Strouhal number is close to the findings of Igarashi [23], but near the bed the Strouhal number shows values smaller than that near the mid depth. It seems that the bed roughness has a decreasing effect on the shedding frequency.

4 Conclusions

In this study, a comparison between the results of flow pattern around a single pier and two piers in tandem was provided using the instantaneous velocities measured by an ADV.

In the gap between the two piers a stronger and considerable upflow (especially in the downstream part of the gap) but a weaker transverse-deflection are formed in comparison with the region behind the single pier. Near the bed, the velocity of flow approaching the downstream pier decreases to $0.2–0.3U_0$ due to the sheltering effect of the upstream pier resulting in a weak wake region. In the wake of the downstream pier, the nature of flow is completely different from that in the wake of the single pier. For the tandem piers, a reattachment regime is formed at the level near the mid-depth and a co-shedding regime near the bed.

The results of power-spectra analysis show that for the single-pier case there is a clearly distinguishable peak at each level with considerable value of $S(f)$, twice as large as that of the two piers at the corresponding levels. Also, for the co-shedding regime near the bed, the two circular piers shed vortices separately at the same frequency. The results show a decrease in the strength of vortical structure in the wake of tandem piers in comparison with a single pier. It seems that the bed roughness has a decreasing effect on the shedding frequency.

The results show further that the high-level turbulence intensities are concentrated near the downstream pier in the tandem-pier cases. The values of turbulence kinetic energy and turbulence intensities show a considerable decrease around the tandem piers in comparison with the single-pier case because it seems that the downstream pier controls the extra turbulence in this region.

Although attempts have been made to take into account all hydraulic considerations for both experiments, a little difference between the approaching-flow conditions may have had some effects on the flow structures which may not have been distinguished from the effects of the configurations of the cylinders.

The experimental results reported provide new understanding of the details of flow behavior around tandem circular cylinders. Further work to examine and extend the results to wider ranges of parameters and geometry are required. These experimental results can appropriately be utilized for validation and benchmarking of numerical models of turbulent flows and then the validated and calibrated numerical models can be used to explore the flow field details for wider ranges of parameters.

Acknowledgements The corresponding author would like to thank Dr. Ali-Asghar Beheshti for his useful and constructive comments during the performance of the experiments. The authors wish to thank the journal editor Professor Wolfgang Rodi for his thoughtful comments and also the anonymous reviewers' constructive comments which helped to improve the final manuscript.

References

1. Ahmed, F., Rajaratnam, N.: Flow around bridge piers. J. Hydraul. Eng. **124**(3), 288–300 (1998)
2. Akilli, H., Akar, A., Karakus, C.: Flow characteristics of circular cylinders arranged side-by-side in shallow water. Flow Meas. Instrum. **15**, 187–189 (2004)
3. Akilli, H., Sahin, B., Tumen, N.F.: Suppression of vortex shedding of circular cylinder in shallow water by a splitter plate. Flow Meas. Instrum. **16**, 211–219 (2005)
4. Ataie-Ashtiani, B., Aslani-Kordkandi, A.: Flow field around side-by-side piers with and without a scour hole. Eur. J. Mech. B, Fluids **36**, 152–166 (2012)
5. Ataie-Ashtiani, B., Beheshti, A.A.: Experimental investigation of clear-water local scour at pile groups. J. Hydraul. Eng. **132**(10), 1100–1104 (2006)
6. Ataie-Ashtiani, B., Baratian-Ghorghi, Z., Beheshti, A.A.: Experimental investigation of clear-water local scour of compound piers. J. Hydraul. Eng. **136**(6), 343–351 (2010)
7. Bearman, P.W., Wadcock, A.J.: The interaction between a pair of circular cylinders normal to a stream. J. Fluid Mech. **61**, 499–511 (1973)
8. Beheshti, A.A., Ataie-Ashtiani, B.: Analysis of threshold and incipient conditions for sediment movement. Coastal Engineering **55**, 423–430 (2008)
9. Beheshti, A.A., Ataie-Ashtiani, B.: Experimental study of three dimensional flow field around a complex bridge pier. J. Eng. Mech. **136**(2), 143–154 (2010)
10. Breusers, H.N.C., Raudkivi, A.J.: Scouring. IAHR Hydraulic Design Manual 2. Balkema, Rotterdam, The Netherlands (1991)
11. Breusers, H.N.C., Niccollet, G., Shen, H.W.: Local scour around cylindrical piles. J. Hydraul. Res. **15**(3), 211–252 (1977)
12. Buffin-Bélanger, T., Roy, A.G.: 1 min in the life of a river: Selecting the optimal record length for the measurement of turbulence in fluvial boundary layers. Geomorphology **68**, 77–94 (2005)
13. Carbonneau, P.E., Bergeron, N.E.: The effect of bedload transport on mean and turbulent flow properties. Geomorphology **35**, 267–278 (2000)
14. Coleman, S.E.: Clearwater local scour at complex piers. J. Hydraul. Eng. **131**(4), 330–334 (2005)
15. Dargahi, B.: The turbulent flow field around a circular cylinder. Exp. Fluids **8**, 1–12 (1989)
16. Dargahi, B.: Controlling mechanism of local scouring. J. Hydraul. Eng. **116**(10), 1197–1214 (1990)
17. Dey, S., Raikar, R.V.: Characteristics of horseshoe vortex in developing scour holes at piers. J. Hydraul. Eng. **133**(4), 399–413 (2007)
18. Ettema, R., Kirkil, G., Muste, M.: Similitude of large scale turbulence in experiments on local scour at cylinders. J. Hydraul. Eng. **132**(1), 33–40 (2006)
19. Ge, L., Lee, S.O., Sotiropoulos, F., Sturm, T.: 3D unsteady RANS modeling of complex hydraulic engineering flows, II: Model validation and flow physics. J. Hydraul. Eng. **131**(9), 809–820 (2005)
20. Graf, W.H., Istiarto, I.: Flow pattern in the scour hole around a cylinder. J. Hydraul. Res. **40**(1), 13–19 (2002)
21. Graf, W.H., Yulistiyanto, B.: Experiments on flow around a cylinder; the velocity and vorticity fields. J. Hydraul. Res. **36**(4), 637–653 (1998)
22. Hannah, C.R.: Scour at pile groups. New Zealand, Christchurch, Univ. of Canterbury, Civil Engineering Dept., Research Rep. No. 28-3 (1978)
23. Igarashi, T.: Characteristics of the flow around two circular cylinders arranged in tandem. Bulletin of JSME **24**, 323–331 (1981)
24. Kim, H.J., Durbin, P.A.: Investigation of the flow between a pair of circular cylinders in the flopping regime. J. Fluid Mech. **196**, 431–448 (1988)
25. Kirkil, G., Constantinescu, S.G., Ettema, R.: Coherent structures in the flow field around a circular cylinder with scour hole. J. Hydraul. Eng. **134**(5), 572–587 (2008)
26. Kirkil, G., Constantinescu, S.G., Ettema, R.: Detached eddy simulation investigation of turbulence at a circular pier with scour hole. J. Hydraul. Eng. **135**(11), 888–901 (2009)
27. Kline, S.J.: Closure to 1983 Symposium on Uncertainty Analysis. J. Fluids Eng. Transactions of the ASME (1985)

28. Landers, M.N., Mueller, D.S.: Channel scour at bridges in the United States. Pub. FHWA-RD-95-184. USDOT, Turner Fairbanks Hwy. Res. Ctr., McLean, Va. (1996)
29. Mahbub Alam, Md., Zhou, Y.: Strouhal numbers, forces and flow structures around two tandem cylinders of different diameters. J. Fluids and Structures **24**, 505–526 (2008)
30. Mahjoub, S.N., Mhiri, H., Bournot, P.H., Le Palec, G.: Experimental and numerical modeling of the three-dimensional incompressible flow behaviour in the near wake of circular cylinders. J. Wind Eng. Ind. Aerodyn. **96**, 471–502 (2008)
31. Melville, B.W., Raudkivi, A.J.: Flow characteristics in local scour at bridge piers. J. Hydraul. Res. **15**(4), 373–380 (1977)
32. Melville, B.W.: Local scour at bridge sites. New Zealand, Auckland, Univ. of Auckland, School of Engineering, Rep. No. 117 (1975)
33. Melville, B.W., Coleman, S.E.: Bridge scour. Water Resources publications LLC, Colirado, USA (2000)
34. Nikora, V., Goring, D.: Flow turbulence over fixed and weakly mobile gravel beds. J. Hydraul. Eng. **126**(9), 679–690 (2000)
35. NorTek, A.S.: ADV Operational Manual. Nortek AS, Vollen, Norway (1996)
36. Oka, S., Kostic, Z.G., Sikmanovic, S.: Investigation of the heat transfer process in tube banks in cross flow. In: International seminar on recent development in heat exchangers, Trogir, Yugoslavia (1972)
37. Ozturk, N.A., Akkoca, A., Sahin, B.: Flow details of a circular cylinder mounted on a flat plate. J. Hydraul. Res. **46**(3), 344–355 (2008)
38. Palau-Salvador, G., Stoesser, T., Rodi, W.: LES of the flow around two cylinders in tandem. J. Fluids Struct. **24**, 1304–1312 (2008)
39. Sahin, B., Ozturk, N.A., Akilli, H.: Horseshoe vortex system in the vicinity of the vertical cylinder mounted on a flat plate. J. Flow Meas. Instrum. **18**, 57–68 (2007)
40. Salim, M., Jones, J.S.: Scour around exposed pile foundations. Compilation of Conf. Scour Papers (1991–1998), ASCE, Reston, Va. (1998)
41. Song, T., Chiew, Y.M.: Turbulence measurement in nonuniform open channel flow using Acoustic Doppler Velocimeter (ADV). J. Eng. Mech. **127**(3), 219–232 (2001)
42. Snyder, W.H., Castro, I.P.: Acoustic Doppler velocimeter evaluation in stratified towing tank. J. Hydraul. Eng. **125**(6), 595–603 (1999)
43. Sumer, B.M., Fredsoe, J.: The Mechanics of Scour in the Marine Environment. World Scientific, Farrer Road, Singapore (2002)
44. Tanida, Y., Okajima, A., Watanabe, Y.: Stability of a circular-cylinder oscillating in uniform flow or in a wake. J. Fluid Mech. **61**, 769–784 (1973)
45. Wahl, T.L.: Analyzing ADV data using WinADV. In: Proc., joint conf. on water resources engineering and water resources planning and management, ASCE, Reston, Va. (2000)
46. Wahl, T.L.: Discussion of despiking acoustic Doppler velocimeter data, by D.G. Goring and V.I. Nikora. J. Hydraul. Eng. **129**(6), 484–487 (2003)
47. Wu, W., Rodi, W., Wenka, T.: 3D numerical modeling of flow and sediment transport in open channels. J. Hydraul. Eng. **126**(4), 4–15 (2000)
48. Zdravkovich, M.M.: The effects of interference between circular cylinders in cross flow. J. Fluids Struct. **1**, 239–261 (1987)